X-ray emission from Seyfert 2 galaxies with optical polarized broad lines

Hisamitsu Awaki[1,2]

Department of Physics, Faculty of Science, Kyoto University

and

Shiro Ueno

Space Utilization Research Program, Tsukuba Space Center, National Space Development Agency of Japan,

and

Yoshiaki Taniguchi

Astronomical Institute, Graduate School of Science, Tohoku University

and

Kimberly A. Weaver

Laboratory for High Energy Astrophysics, NASA Goddard Space Flight Center,

ABSTRACT

We analyze the $0.5-10$ keV spectra of six Seyfert 2 galaxies observed with the X-ray satellite ASCA: Mrk 3, Mrk 348, Mrk 1210, Mrk 477, NGC 7212, and Was 49b. These galaxies were selected based on their possession of optical polarized broad lines. In the $2-10$ keV band, their spectra are heavily absorbed, with $2-10$ keV absorption-corrected X-ray luminosities ranging from 10^{42} to 10^{43} ergs s^{-1}. The observed X-ray emission is generally only about one tenth that predicted based on their known infrared and Hβ luminosities. This apparent X-ray weakness can be understood if a considerable fraction of the nuclear activity is completely blocked from view by thick matter along our line of sight to the nucleus.

All of these galaxies possess significant soft X-ray emission whose origin appears to be scattered light from their nuclear emission. Based on this hypothesis, we estimate a typical scattering efficiency for X-rays to be about 10%. This efficiency is larger than the few % found for ordinary Seyfert 2 galaxies with no report of optical polarized broad lines. A large scattering efficiency is best explained by an apparent weakness of the hard X-ray luminosity rather than unusually strong scattered light in the soft band. When we estimate the scattering efficiency using the intrinsic luminosity derived assuming

[1]CREST: Japan Science and Technology Corporation (JST), 4-1-8 Honmachi, Kawaguchi, Saitama 332

[2]present address: Department of Fundamental Material Science, Faculty of Science, Ehime University, Matsuyama, 790-8577, Japan

Compton scattering dominates the hard X-ray spectrum, as opposed to a purely absorbed nuclear continuum, the efficiency can be less and is similar to that of ordinary Seyfert 2 galaxies. Since the difference between our sample and ordinary Seyfert 2 galaxies can be explained by the difference of viewing angle, the similar scattering efficiency suggests the existence of a scattering region that is larger than the putative dusty torus.

Subject headings: galaxies: active— galaxies: Seyfert—X-rays: galaxies

1. INTRODUCTION

Seyfert galaxies are nearby active galaxies that have been traditionally classified into two types according to the presence or absence of broad optical/UV emission lines (more than a couple thousand km s^{-1} FWHM). However, after broad lines were discovered in the polarized spectrum of the typical Seyfert 2 galaxy, NGC 1068 (Antonucci & Miller 1985), it became clear that broad-line region clouds can exist in Seyfert 2 galaxies as well as Seyfert 1s, although these clouds may be located inside (and hidden behind) an optically and geometrically thick disk. With the development of better instruments and techniques, spectropolarimetry has revealed the existence of polarized broad emission lines (and hence hidden BLRs) from more than ten Seyfert 2 galaxies (e.g. Miller & Goodrich 1990, Tran, Miller, & Kay 1992).

Based on these polarized Seyfert 2 galaxies, a viewing-dependent unification scenario has been proposed that predicts the existence of a hidden active nucleus and broad line region in all Seyfert galaxies, making Seyfert 1 and 2 galaxies are essentially identical. Hard X-ray observations with the Japanese X-ray satellite Ginga revealed hidden luminous nuclei in several Seyfert 2 galaxies (e.g. Awaki et al. 1991), demonstrating that hard X-ray observations are useful to reveal highly obscured nuclei. Since nuclear X-rays pass though the thick matter, such galaxies are the best targets to investigate AGN environments. In particular, it is crucial to reveal the origin of the weak excess emission in the soft X-ray band (e.g. Krupper, Urry & Canizares 1990). One possibility is that the soft X-rays represent scattered light, similar to optical polarized broad lines (Netzer, Turner & George 1998). Another possibility is that soft X-rays can come from starbursts (e.g., Dahlem, Weaver & Heckman 1998) or AGN-driven jets (Colbert et al. 1998).

If X-ray and optical/UV photons are scattered in the same way, there should be a relation between them. To investigate whether the soft X-ray emission in Seyfert 2 galaxies is related to nuclear activity, we examine those known to have optical polarized broad emission lines. Choosing objects with significant polarization maximizes the chance of detecting scattered X-rays from the AGN as opposed to X-rays from the galaxy. The Japanese X-ray satellite ASCA allows spectroscopy in the entire $0.5-10$ keV band, and so we can directly measure both the hard X-ray emissions from obscured nuclei and any associated soft X-ray emission. By comparing our X-ray results with those of optical spectropolarimetric observations, we can test the origin of the soft component and investigate the properties of the nuclei and scattering regions in Seyfert 2 galaxies with polarized broad lines (hereafter PBL Seyfert 2 galaxies). The differences between the amount of polarization in PBL Seyfert 2 galaxies compared to more typical Seyfert 2 galaxies that have no detectable polarization, should affect their corresponding X-ray properties. We attempt to clarify this difference in our analysis.

2. TARGET SELECTION AND DATA REDUCTION

Miller & Goodrich (1990) and Tran, Miller & Kay (1992) found about 10 PBL Seyfert 2 galaxies. Eight of these have been observed with ASCA. ASCA data for NGC 1068, Mrk 463E and the first observation of Mrk 3 have been reported by Ueno et al (1994), Ueno et al. (1996) and Iwasawa et al. (1994), respectively. We refer to these papers for these three objects, and we analyze the other five Seyfert 2 galaxies (Mrk 348, Mrk 477, Mrk 1210, NGC 7212, Was 49b) and the second observation of Mrk 3.

ASCA (Tanaka, Inoue, & Holt 1994) has four focal-plane detectors: two solid-state imaging spectrometers (called here SIS 0 and SIS 1) and two gas imaging spectrometers (called GIS 2 and GIS 3). The SIS and GIS operate simultaneously. In our observations, the SIS data were taken with the instrument in 1-CCD FAINT mode at all bit-rates. The GIS data were obtained in PH mode at all bit-rates. The field of view of SIS 1-CCD mode and GIS are $11'$ square, and $40'$ diameter, respectively.

We select data using the following data filtering,

COR $>$ 4 GeV c^{-1}, ELV $>$ 5 deg, and T_SAA $>$ 60 s,

where COR is cutoff rigidity, ELV is target elevation from Earth's rim and T_SAA is the time after passage through the South Atlantic Anomaly. In order to reject contaminating X-rays from Earth's rim, data are also filtered using the angular distance from Earth's rim during daylight (BR_EARTH). For Mkn 3, we accept data with BR_EARTH $>$ 35 deg and for the other targets, we accept data with BR_EARTH $>$ 10 deg. The observation log and the exposure times after filtering are listed in Table 1.

We accumulate SIS0 and SIS1 data within a $6'$ diameter circle centered on the X-ray source; background spectra are taken from a non-source region $> 8'$ in diameter. For the GIS, we sum data from GIS2 and GIS3 in an $8'$ diameter circle centered on the X-ray source; background spectra are taken from an annulus with $12'$-$32'$ diameter centered on the X-ray source. We find several X-ray sources in the background region and exclude contaminating sources with $8'$ (for SIS) and $12'$ (for GIS) diameter circles. The count rates after background subtraction are listed in Table 1.

In the field of Was 49b, there is a bright source, RX J1214.4+2936, located $4'.6$ away from the target galaxy (Appenzeller et al. 1998). Although this source is classified as a Seyfert 2 galaxy at redshift of 0.307, the X-ray characteristics are similar to that of a Seyfert 1 galaxy or a QSO, i.e. the spectrum is described by a single power-law model with a photon index of 1.30±0.15 and an absorption column of less than 6×10^{20} cm^{-2}. The X-ray flux is $\sim8\times10^{-13}$ ergs s^{-1} cm^{-2} in the $2-10$ keV band, which corresponds to an X-ray luminosity of $\sim4\times10^{44}$ ergs s^{-1}. The amount of contamination from this source is estimated to be only 10±2% of the X-ray flux of Was 49b in the $0.5-2$ keV band, and so it should not seriously affect our analysis.

For Mrk 477, Mrk 1210, and NGC 7212, which were observed twice, we first analyze the two observations separately. Table 1 shows the count rate in the $0.5-10$ keV band for each. Since their count rates do not vary significantly and their hardness ratios of $2-10$ keV versus $0.5-2$ keV rate remain the same to within a 1 σ error, we conclude that their X-ray spectra do not change significantly between the two observations. As a result, the separate observations are added to produce one spectrum for each galaxy for analysis purposes.

We combine energy bins to contain more than 40 counts in each bin and apply a χ^2 method in the XSPEC package for spectral fitting.

3. SPECTRAL ANALYSIS AND RESULTS

The X-ray spectra of Seyfert 2 galaxies can be approximated by equation (1), which represents a two-component continuum plus an Fe Kα line (e.g. Turner et al. 1997a). We apply this model, labeled model 1, in our fitting procedure, with a power-law as the soft X-ray component to represent the contribution of scattered emission from the AGN. Some broadening of the Fe K line is reported by Turner et al. (1997a), but it is unclear whether there is significant line broadening in our data. We thus assume that the Fe K line is narrow for all cases. Model 1 describes all sources well with a reduced χ^2 $\sim$1. The fitting results are listed in Table 2, and the spectra are shown in Figure 1.

$$I(\mathrm{photon\ s^{-1}cm^{-2}keV^{-1}}) = \exp(-N_{\mathrm{H0}}\sigma_{\mathrm{abs}}) \times (\mathrm{soft\ component} + \exp(-N_{\mathrm{H1}}\sigma_{\mathrm{abs}})\ (A\ E^{-\Gamma} + \mathrm{line})), \tag{1}$$

where the soft component is a power-law in models 1, 2, and 3 and a Raymond plasma in model 4.

For model 1, the observed $2-10$ keV fluxes for the hard components range from 3×10^{-13} to 1.8×10^{-12} ergs s^{-1} cm^{-2}, which correspond to observed luminosities (L^{obs}_{2-10}) of $10^{42}-10^{43}$ ergs s^{-1} assuming $H_0 = 50$ km s^{-1} Mpc^{-1} (see Table 3).

3.1. The hard X-ray components

Hard X-ray emission with Γ $\sim$2 is often seen in normal galaxies (e.g. Okada 1998) and is thought to originate from a superposition of discrete sources (e.g. low mass X-ray binaries and SNe; Makishima et al. 1989). It is well known that the ratio of X-ray to blue band luminosities (L_{B}) is about 4×10^{-5} for normal and starburst galaxies (e.g. Awaki 1999), i.e. the luminosity from the superposition of discrete sources is estimated to be 1.5×10^{39} $(L_B/10^{10}L_\odot)$ ergs s^{-1} in the $2-10$ keV band. Since L_{B} for our sample is order $10^{10}L_\odot$ (Whittle et al. 1992), we conclude that the hard X-ray emission is most likely to originate from nuclear activity.

When applying model 1, the photon indices of the hard component are poorly determined, ranging from -0.14 to 2.22. Assuming the hard emission is related to the AGN, we next fix the photon index of the hard component to be 1.7 (model 2), which is the canonical observed value for type 1 AGNs (e.g. Mushotzky 1982). When the best fit value of N_{H0} is less than the galactic absorption, we set N_{H0} equal to the galactic column.[3] The equivalent width of the Fe Kα line is the most important parameter to investigate the origin of the hard component (e.g. Awaki et al. 1991 and Turner et al. 1997b), and so we fix the center

[3]obtained from EOLS/EINLINE V 2.4 at Smithsonian Astrophysical Observatory.

energy of the line at 6.4 keV (in the rest frame), the energy of Fe Kα fluorescence from cold matter.

When fixing the hard X-ray photon indices (model 2), the values of χ^2 increase because the overall spectra tend to be flatter than a $\Gamma \sim$1.7 spectrum. However, if our assumptions about the intrinsic spectral shape of the hard X-ray (AGN) component are correct, then model 2 implies large column densities and large equivalent widths for the Fe Kα line (see Table 2). The absorption corrected $2-10$ keV luminosities for the hard component are greater than 10^{42} ergs s^{-1} (see Table 4; hereafter $L^{\rm ac}_{2-10}$ denotes this absorption corrected luminosity). $L^{\rm ac}_{2-10}$ is useful to compare with results in the literature.

We found that some galaxies have indices from 0 to 1 in model 1, which are smaller than the canonical Seyfert 1 value of $\sim$1.7. Matt et al. (1996) point out that, besides absorption, a flat spectrum can result from a significant Compton reflection component. To test this idea, we apply a Compton reflection model (model 3) to the hard components of Mrk 1210, Mrk 477, Was49b and NGC 7212 and find that the hard X-ray emission can be reproduced by Compton reflection (Table 2). The χ^2 values are less than those for the absorbed power-law model (models 1 and 2), although iron line intensities are much weaker than predicted for reflection by Reynolds et al. (1994) and Matt et al. (1996).

3.2. The Soft X-ray components

For a power-law description of the soft X-ray emission we find observed 0.5 to 2 keV fluxes of about 10^{-13} ergs s^{-1} cm^{-2} and photon indices of $\Gamma \sim$1-2. Absorption in excess of the galactic column is not indicated for most galaxies. The X-ray luminosities for the soft components are listed in Table 4.

In order to test the origin of the soft component, we characterize it using the Raymond-Smith plasma model (Raymond & Smith 1977) (model 4). We set the metal abundance free, because the thermal emission detected from starburst galaxies and NGC 1068 can be reproduced by a thin thermal plasma model with sub-solar abundances (e.g. Ueno et al. 1994 for NGC 1068, Tsuru et al. 1997 for M82). We find the temperatures for NGC 7212 and Mrk 477 to be greater than several keV, while the temperature and metal abundance for Mrk 1210 and Was 49b are 0.86 keV and 0.03, and 0.72 keV and 0.02, respectively.

It is known that some Seyfert 2 galaxies possess line-like structures around 0.9 keV (e.g. Hayashi et al. 1996 for NGC 2110, Comastri et al. 1998 for NGC 4507). Line emission is important to investigate the origin of the soft component, because highly ionized neon (Ne IX), and fully ionized oxygen make a line-like structure at about 0.9 keV (e.g. Netzer 1995). We examined the line emission around 0.9 keV adding a narrow line to model 2. Line-like features are apparent in the spectra of Mrk 3 and Mrk 477 (Table 5). The detection of the line in the spectrum for Mrk 3 is consistent with the result by Griffiths et al. (1998).

4. DISCUSSION

4.1. The Hard Component

4.1.1. Nuclear Activities in Seyfert 2 Galaxies with Polarized Broad Lines

Based on our spectral fits, we find hard X-ray emission associated with nuclear activities in PBL Seyfert 2 galaxies. For an absorbed power-law model with a photon index of 1.7 (our model 2), we infer X-ray activities with $L^{\rm ac}_{2-10} > 10^{42}$ ergs s^{-1} obscured by thick matter with column densities of $\sim 10^{23}$ cm^{-2}. Assembling the available X-ray results for other PBL Seyfert 2 galaxies, (NGC 1068; Ueno et al. 1994, NGC 7674; Malaguti et al. 1998, and Mrk 463E; Ueno et al. 1996), obscured nuclei are detected in all PBL Seyfert 2 galaxies observed to date in the hard X-ray band. We conclude that obscured nuclei are common in PBL Seyfert 2 galaxies.

Using $L^{\rm ac}_{2-10}$, we can examine whether the estimated number of photons are sufficient to ionize the surrounding region. For Seyfert 1 galaxies, the X-ray luminosity in the $2-10$ keV band ($L_{\rm X}$) is well correlated with the broad $H\beta$ luminosity ($L_{{\rm H}\beta}$), with a ratio of $L_{\rm X}/L_{{\rm H}\beta} \sim 10-100$ (e.g. Blumenthal, Keel, & Miller 1982). Figure 2 shows this correlation for Seyfert 1 galaxies and QSOs, quoted from Padovani & Rafanelli (1988) and Malaguti, Bassam, & Caroli (1994), respectively (solid circles). If Seyfert 2 galaxies are Seyfert 1s viewed edge-on, their intrinsic properties should be the same as Seyfert 1s. We test this idea by plotting the PBL Seyfert 2 galaxies (open circles) in Figure 2, estimating $L_{{\rm H}\beta}$ from the polarized $H\beta$ flux, τ=0.1, $\Delta\Omega/4\pi$=0.1, and known polarization degree (Miller & Goodrich 1990, Tran 1995a). It is clear that $L^{\rm ac}_{2-10}$ for PBL Seyfert 2 galaxies lies systematically below the relation for Seyfert 1 galaxies and QSOs, such that there are 10 times fewer ionizing photons than expected, assuming our estimate of $L_{\mathrm{H}\beta}$ is correct. The discrepancy is similar for other indicators of nuclear activity; $L^{\mathrm{ac}}_{2-10}/L_{\mathrm{IR}}$ for PBL Seyfert 2 galaxies are only 1/10 that of Seyfert 1 galaxies (Figure 3a)[4], and Bassani et al. (1999) point out a small ratio of L^{ac}_{2-10} to the luminosity of [OIII]. We conclude that correcting only for hard X-ray absorption results in PBL Seyfert 2 galaxies having L^{ac}_{2-10} that is 10 times less than predicted if they harbor a Seyfert 1 nucleus.

4.1.2. Weak Activity?

If models 1 or 2 do not represent the actual spectral form of the nuclear source, L^{ac}_{2-10} does not represent the true luminosity. We found that the X-ray spectra for some PBL Seyfert 2s are well represented with the Compton reflection models, although their iron emission lines are weaker than that for a pure reflection model (e.g. Matt et al. 1996). Since most of the iron emission in this scenario is attributed to the reflection component, the contribution of reflection to the hard component can be estimated from a ratio of the measured to predicted iron line intensities. Assuming the equivalent width of 1.5 keV for a pure reflection component, the contribution is estimated to be $20-50\%$. From theoretical considerations, the upper limit to the efficiency of the Compton mirror in the 2–10 keV band is about 7% for $\Delta\Omega/2\pi = 1.0$. If we assume an efficiency of 5%, the true X-ray luminosity ($L^{\mathrm{intrinsic}}_{2-10}$) is described as

$$L^{\mathrm{intrinsic}}_{2-10} = 20 \times L^{\mathrm{ac}}_{2-10}(\frac{EW}{1500eV})(\frac{Eff_{\mathrm{Compton}}}{0.05})^{-1}, \tag{2}$$

where EW and $\mathrm{Eff}_{\mathrm{Compton}}$ are the observed equivalent width of iron Kα line and the efficiency of the Compton mirror in the 2–10 keV band respectively. Figure 3b shows a plot of $L^{\mathrm{intrinsic}}_{2-10}$ versus L_{FIR}. PBL Seyfert 2 galaxies have the same ratio of $L^{\mathrm{intrinsic}}_{2-10}/L_{\mathrm{FIR}}$ as Seyfert 1s. Therefore, by accounting for the observed spectrum as reflected rather than absorbed emission, the intrinsic source would be ten times more luminous and PBL Seyfert 2 galaxies would be consistent with having powerful AGN activity. Tran 1995b pointed out the existence of strong nuclear activities in NGC 7212 and Mrk 463E from the line ratio diagnostic of jet regions. The powerful activities inferred from the X-ray data after the correction of reflection efficiency are consistent with his claim.

4.1.3. Time Variability

Seyfert 1 galaxies with X-ray luminosities of 10^{43} ergs s^{-1} have variability time scales of 10000 seconds. If PBL Seyfert 2 galaxies possess obscured Seyfert 1 type nuclei but we are seeing their hard X-ray emission directly, similar time variability is expected. However, Mrk 1210, Mrk 477 and NGC 7212 show no significant time variability in periods of one month, one day and one week, respectively. This probably indicates that these galaxies do not have small variability time scale such as Seyfert 1 galaxies, although we need more X-ray monitors in order to achieve the conclusion. Mrk 3 has been monitored with the Einstein, Ginga, BBXRT, ROSAT and ASCA X-ray missions. Figure 4 shows light curves in the soft and hard bands. As Marshall et al. (1991) and Iwasawa et al. (1994) mentioned, the hard X-ray flux gradually decreases between the Ginga and ASCA observations. The variability time scale is about 1 yr, which is similar to that of luminous QSOs.

A lack of short timescale spectral variability for PBL Seyfert 2 galaxies can be explained by more massive black holes with smaller accretion rates and/or the dominance of the Compton reflection process for energies approaching 10 keV. The latter indicates more powerful X-ray activity, and so both possibilities suggest the existence of more massive black holes than those of Seyfert 1 galaxies with the same apparent X-ray luminosity. This result is consistent with arguments by Nishiura & Taniguchi (1998), who deduced large central black hole masses from analysis of line widths of polarized broad lines.

4.2. The Soft X-ray Component

4.2.1. The Origin of the Soft component

We detect distinct soft X-ray components with X-ray luminosities in the $0.5-2$ keV band of about 10^{41} ergs s^{-1}. No associated strong absorption indicates that the X-rays originate outside the thick matter that absorbs the hard X-rays. The soft X-rays can be associated with circumnuclear starburst activities which are often seen in Seyfert 2 galaxies (e.g. Maiolino & Rieke 1995). On the other hand, optical scattered light is observed by spectropolarimetry. From the analogy of these observations, it is naturally

[4]The IRAS color for PBL Seyfert 2 galaxies are warm (log ($F_{25\mu\mathrm{m}}/F_{60\mu\mathrm{m}}$ >-0.5), which indicates that the dominant energy source of IR emission is AGN activity.

suggested that X-rays from nuclei are also scattered into our line of sight. We examine possibilities for the origin of the soft component using 1) the X-ray spectrum, 2) the correlation between Lx and $L_{\rm FIR}$, and 3) the correlation between Lx and luminosities of scattered $H\beta$ lines.

The X-ray spectrum: we tried to fit the soft components with either the absorbed power-law model (models 1 and 2) or the thin thermal plasma model (model 4). NGC 7212, Mrk 477, Mrk 3, and Mrk 348 have flat spectra represented by a power-law model with a photon index < 2.3. This result, combined with little soft X-ray absorption, suggests that thermal emission due to starburst activity is not dominant in the soft X-ray band. In addition, we detect a line-like feature around 0.9 keV for Mrk 3 and Mrk 477, which is one characteristic of a scattered light in a highly ionized plasma region (Netzer 1995, Griffiths et al. 1998).

On the other hand, Mrk 1210 and Was 49b have softer spectra than those of the other targets. Their soft components can be described as thin thermal emission with low metal abundances of <0.1 and <0.14 having kT ∼0.86 keV and kT ∼0.72 keV, respectively. For Mrk 463E, Ueno et al (1994) report a thermal soft X-ray component with kT ∼1 keV. Since Mrk 463E and Was 49b are galaxy-margers, there is a possibility of on-going starburst activity. However, there are no reports on the existence of powerful starburst activities in their nuclear regions, and their infrared colors (log $F_{25\mu\rm m}/F_{60\mu\rm m}$) in the IRAS band are about 0. Therefore, we consider that most soft X-rays are associated with their AGN activities. We note that a possibility of the starburst origin can not be ruled out from our spectral analysis alone.

$L_{\rm FIR}$ vs $L_{\rm X}$: the X-ray luminosities of optically thin thermal emission from starburst galaxies and normal galaxies are well correlated with far infrared luminosity. David, Jones & Forman (1992) found the strong correlation with $L_{\rm FIR}/L_{\rm X}$ ∼2000 in the 0.5–4.5 keV band from a detail analysis for a large number of galaxy samples observed by Einstein. Figure 5 presents our sample. We find that most Seyfert 2 galaxies have excess soft emission, and that the contribution of the starburst component is estimated to be less than 50% except for NGC 1068. We note that NGC 1068 is a luminous infrared source with powerful starburst activity. Thus, the soft components for our target galaxies are most likely to originate from their AGN activities rather than starburst activities.

$L_{\rm H\beta}$ vs $L_{\rm X}$: it is known that the X-ray luminosities of Seyfert 1 galaxies are well correlated with $L_{\rm H\beta}$ (Blumenthal, Keel, & Miller. 1982) because broad $H\beta$ lines are emitted from photoionized regions. If the broad $H\beta$ lines and nuclear light are scattered in the same region, the luminosity of the scattered $H\beta$ lines should correlate with that of the scattered X-ray component. Figure 6 shows a correlation of the soft component and the scattered broad $H\beta$ line luminosities ($L_{\rm H\beta\_scat}$) for our sample. The $L_{\rm H\beta\_scat}$ were estimated using eq.(3.1) in Tran (1995b). The two solid lines in Figure 6 show an extrapolation from the relation found in Seyfert 1 galaxies (see section 4.1). Considering the uncertainty of polarization degree, the objects in our sample lie in the area of Seyfert 1 galaxies. The consistency of properties between our sample and Seyfert 1 galaxies indicates that most of the soft X-rays in PBL Seyfert 2 galaxies can be explained by scattered light, and that electron scattering dominates dust scattering for our sample. This result is consistent with early work by Tran (1995b).

From these relevant considerations, we conclude that soft X-rays in PBL Seyfert 2 galaxies originate mostly from scattered light. We note that Heckman et al. (1997) point out that Mrk 477 has a powerful nuclear starburst with a bolometric luminosity of $3 \times 10^{10} - 10^{11} L_{\odot}$. The luminosity due to the starburst activity is comparable to that of the AGN activity, however it appears to be dominated by the AGN in soft X-rays (Levenson, Weaver and Heckman, in prep.). Using the ratio of $L_{\rm FIR}/L_{\rm X}$ for starburst galaxies, the contribution of the starburst activity in the soft band is estimated to be about 10^{40} ergs s^{-1}, which is about 10% of the observed luminosity. Therefore we conclude that we can ignore the contribution of the starburst activity in Mrk 477.

4.2.2. Scattering Efficiency of the Warm Mirror

Using the wide band ASCA spectra, we can estimate the scattered and intrinsic X-ray luminosities at the same time. If scattered light dominates the soft X-ray component for PBL Seyfert 2 galaxies, we can use the ratio of normalizations between the soft and the hard components to indicate the scattering efficiency in the scatterers. To do this for the continuum spectra, we set Γ(soft) equal to Γ(hard). However, there are several spectral lines in the scattered component (e.g. Netzer 1997). Since ASCA can not separate the lines from the continuum, we also test the method of not setting Γ(soft) equal to Γ(hard). For this case, we determine the intrinsic luminosity in the $0.5-2$ keV band by assuming a power-law model with Γ=1.7, extrapolating this model to lower energies and calculating the flux. The conversion factor determined by extrapolating the luminosities is deduced to be 0.55, which allows us to obtain the scattering efficiency. We note that these scattering efficiency is consistent with those deduced from the ratio of the normalizations within 20%. The scattering efficiency results from an optical depth(τ_{es}) of a scattering medium multiplied by a covering factor of the scatterer($\Delta\Omega$).

$$(scattering\ \ efficiency) = \frac{L_{\rm scat}}{L_{\rm intrinsic}} \sim \frac{L_{0.5-2}^{\rm soft}}{L_{0.5-2}^{\rm intrinsic}}, \quad (3)$$
$$\sim \tau_{es} \times \frac{\Delta\Omega}{4\pi}$$

The τ_{es} is given by the column density ($N_{\rm H}^{\rm scat}$) in the scattering region multiplied by the Thomson scattering cross section. For the hard component, we infer that the true AGN activity is greater than $L_{2-10}^{\rm ac}$. We define B as the ratio $L_{2-10}^{\rm intrinsic}/L_{2-10}^{\rm ac}$. From eq.(3), $N_{\rm H}^{\rm scat}$ is calculated by the following relation,

$$N_{\rm H}^{\rm scat} \sim 1 \times 10^{24}\ (\frac{\frac{\Delta\Omega}{4\pi}}{0.133})^{-1}\ (\frac{\frac{L_{0.5-2}^{\rm soft}}{L_{0.5-2}^{\rm ac}}}{0.1})\ B^{-1} \quad ({\rm H/cm^2}). \quad (4)$$

The upper panel in Figure 7 shows the distribution of $L_{0.5-2}^{\rm soft}/L_{0.5-2}^{\rm ac}$. The points concentrate around 10%. Taking the ratio to be 0.1, the column density in the scattering region is calculated to be $10^{24}B^{-1}$ cm^{-2}, when the covering factor is 0.133, which corresponds to the opening angle of the torus of 60 degrees. The analysis of the hard X-ray component supports the large-B case. For example, for B=10, the column is estimated to be 10^{23} cm^{-2}, which is less than or comparable to those of our line of sight. The optical depth (τ_{es}) of the scatterer is deduced to be ∼0.06, which is similar to those used in the analysis of PBL Seyfert 2 galaxies (e.g. Miller & Goodrich 1990).

We can also estimate the location of the scattering medium. From eq. (4), the column density in the scattering region is $10^{24}B^{-1}$ cm^{-2}. If the scatterer were cold, the soft X-rays would be absorbed by carbon and oxygen. We do not observe a low-energy cut off and so carbon and oxygen must be ionized in the scatterer. Kallman & McCray (1982) pointed out that for log $\xi > 2$, the population of fully ionized carbon and oxygen is ∼100 % and >30%, respectively, where ξ is the ionization parameter with the relation of $\xi = L/(n_{\rm e}R^2)$. In log$\xi > 2$, the electron temperature is greater than 10^5 K (Kallman & McCray 1982), which is roughly consistent with the prediction with spectropolarimetry (e.g. Tran 1995b). The ionization parameter,ξ, is calculated from the observed value (see Eq. (5)), i.e. X-ray luminosity and column density of the scatterer.

$$\xi = 30\ (\frac{L_{0.5-2}^{\rm ac}}{10^{43}{\rm ergss^{-1}}})\ (\frac{N_{\rm e}}{10^{24}{\rm cm^{-2}}})^{-1}(\frac{R}{1{\rm pc}})^{-1}\ B. \quad (5)$$

To obtain a large ξ, the scatterer should be located within 0.3 pc for B=1 and within 30 pc for B=10. For the most probable dusty torus model for Seyfert nuclei (e.g. Murayama, Mouri, & Taniguchi 2000), the full height of the torus is estimated to be $0.3-1.5$ pc. Assuming B=1, the scatterer is located within the torus, while for B=10, the scatterer is located outside the torus. Since large B is more likely from the analysis of the hard component, the scattering region should be larger than that of the dusty torus.

Variability restricts the size of an emitting region. For Mrk 3, long-term monitoring for 10 years shows that although the hard component changed by a factor of 6 during 3 years, no decrease of the soft component was seen. If most of the soft X-rays from Mrk 3 are scattered, the flux of the soft component should decrease within the light travel time from the nucleus to the scattering region. The large time lag indicates that the distance of the scatterer from the nucleus is comparable to 6 light years (∼ 2 pc). This result supports a large scattering region. Continuous monitoring of Mrk 3 in the X-ray band is crucial to verify the location of the scattering region.

4.2.3. Comparison with Other Seyfert 2 Galaxies

Ueno (1995) estimate a ratio of $L_{0.5-2}^{\rm soft}/L_{0.5-2}^{\rm ac}$ for Seyfert 2 galaxies without reports of polarized broad lines using the ratio of the normalization of their soft and hard components (Table 4). For comparison, we show a histogram of $L_{0.5-2}^{\rm soft}/L_{0.5-2}^{\rm ac}$ for Seyfert 2 galaxies with and without reports of polarized broad lines (Figure 7). For typical Seyfert 2s, the ratios tend to be less than those of PBL Seyfert 2 galaxies. This is explained either by a stronger soft component or a weaker hard component in PBL Seyfert 2 galaxies. To examine which applies, we compare $L_{2-10}^{\rm ac}$-$L_{\rm FIR}$ for both types, assuming that $L_{\rm FIR}$ represents the real nuclear activities because their infrared colors are warm except NGC 1068 (as discussed above). Figure 8a shows a color-color diagram of $L^{\rm soft}_{0.5-2}/L^{\rm ac}_{0.5-2}$ and $L^{\rm ac}_{2-10}/L_{\rm FIR}$. Closed circles and open circles represent PBL Seyfert 2 and other Seyfert 2 galaxies, respectively. When the absorption correction is applied, there is a clear separation of the two types of Seyfert 2 galaxies. For the reflection correction, using $L^{\rm intrinsic}_{0.5-2}$ in place of $L^{\rm ac}_{0.5-2}$ (Figure 8b), the data are all concentrated in the same region, since PBL Seyfert 2s have larger $L^{\rm ac}_{0.5-2}/L^{\rm intrinsic}_{0.5-2}$ ratios than those of other Seyfert 2 galaxies. This result indicates that the distributions of $L^{\rm soft}_{0.5-2}/L^{\rm intrinsic}_{0.5-2}$ in Figure 7 are due to underestimation of their nuclear activities, and that the scattering efficiencies of PBL Seyfert 2 galaxies are similar to those of other Seyfert 2 galaxies, which is a few %.

4.2.4. Interpretation on PBL Seyfert Galaxies

We find that the ratios of $L^{\rm ac}_{2-10}/L_{\rm FIR}$ of PBL Seyfert 2 galaxies are different from those of other Seyfert 2 galaxies. We propose that the difference is caused by viewing angle. First, about half of our PBL Seyfert 2 galaxies were selected among Seyfert 2 galaxies with high polarization degrees as mentioned by Miller & Goodrich (1990). If the scattering region is larger than the torus, most of the scattering region is not obscured. The polarization degree (P) is described by the function of the viewing angle (i), $P = \sin^2 i/(2\alpha + \sin^2 i)$, where α is the value derived from cone angle of the torus (see Miller & Goodrich 1990 in detail). The difference in the amount of polarization is explained as other Seyfert 2 galaxies having smaller viewing angles than PBL Seyfert 2 galaxies. Next, the contribution of the Compton reflection component in the $2-10$ keV band probably depends on the viewing angle, because most Seyfert 2 galaxies with pure reflection in the $2-10$ keV band have an H_2O maser line which is explained by their edge-on geometry (e.g. Matt et al. 1999 for the circinus galaxy, Ueno et al. for NGC 1068, Iwasawa et al. for NGC 4945). Furthermore, Bassani et al. (1999) find an anti-correlation between iron line equivalent width and $F_{\rm X}/F_{\rm [OIII]}$ for a large sample including Seyfert 1 galaxies and Seyfert 2 galaxies with the H_2O masers.

We suggest that the X-ray properties can be smoothly connected from Seyfert 1 galaxies to Seyfert 2 galaxies with the H_2O masers lying between "typical" Seyfert 2 galaxies and PBL Seyfert 2 galaxies. We conclude that the separation seen in Figure 8a results from smaller $L^{\rm ac}_{2-10}/L_{\rm FIR}$ for PBL Seyfert 2 galaxies, and that $L^{\rm ac}_{2-10}/L_{\rm FIR}$ decreases as the viewing angle increases. Our picture is consistent with the fact that the viewing angle of Mrk 348 is smaller than the other PBL Seyfert 2 galaxies (Tran 1995b). Heisler, Lumsden, & Bailey (1997) proposed that PBL Seyfert 2 galaxies have smaller viewing angle than other Seyfert 2 galaxies from the analysis of their extinction,$E(B-V)$. However X-ray properties suggest that the scattering region is larger than the torus, and that PBL Seyfert 2 galaxies have larger viewing angle than other Seyfert 2 galaxies.

We consider two possibilities to explain the viewing angle dependence of $L^{\rm ac}_{2-10}/L_{\rm FIR}$; 1) anisotropic radiation from the Seyfert 2 nucleus due to X-ray beaming and 2) the existence of thick, clumpy clouds that block a considerable fraction of X-ray photons in the $2-10$ keV band (Figure 9). In the former model, anisotropic radiation can result from a jet structure found in radio band (Ulvestad & Wilson 1984). The latter model is referred to as the dual absorption model (Weaver et al. 1994), in which absorption columns are $N_{\rm H}$ $\sim$$10^{23}$ and $> 10^{24}$ for PBL Seyfert 2 galaxies. Since this model indicates the some fraction of the X-rays are not absorbed by a thick matter, the thick matter should be smaller than the size of X-ray emitting region. In NGC 4258, it is found that H_2O vapor masing clouds are very small, thick clouds located in its central nuclear region (Miyoshi et al. 1995). Thus the masing cloud is one candidate of the thick matter found in our observations. Although we have proposed two possibilities, we have not obtained conclusive result on this issue, because we only obtained the $0.5-10$ keV spectra with poor statistics. This is a subject for future missions with large effective area and high energy resolution, such as XMM, Astro-E, Constellation-X, and XEUS.

5. CONCLUSION

We analyze the X-ray data for Seyfert 2 galaxies which have polarized broad lines in the optical band.

All galaxies show obscured nuclear activities with $2-10$ keV absorption-corrected luminosities of $10^{42}-10^{43}$ ergs s^{-1}. However, absorption corrected X-ray luminosities ($L^{\rm ac}_{2-10}$) are less than expected based on predictions from $L_{\rm FIR}$, $L_{\rm H\beta}$ using relations found in Seyfert 1 galaxies. We examine whether the small X-ray luminosities are real or not, and find that this can be explained if the effects of Compton reflection rather than absorption dominate the $2-10$ keV spectra. In this case, the intrinsic X-ray luminosities are consistent with the higher luminosities expected from the amount of reflection.

Soft X-ray emission is detected in all galaxies. The X-ray spectrum and correlation of $L_{\rm FIR}$-$L^{\rm soft}_{0.5-2}$ and $L_{\rm H\beta\_scat}$-$L^{\rm soft}_{0.5-2}$ reveal that most X-rays in the soft component are scattered light by a warm scatterer. The typical scattering efficiency derived from the ratio of the soft to apparent hard band luminosity is about 10%; larger than that of Seyfert 2 galaxies without polarized broad lines. This discrepancy can result from an underestimation of intrinsic activity. The scattering efficiencies deduced from real activities are similar to those of other Seyfert 2 galaxies, which are a few %. The small scattering efficiency supports the existence of a large scattering region, as opposed to the compact scattering region proposed by Hisler, Lumsden, & Bailey (1997).

We suggest that PBL Seyfert 2 galaxies have larger viewing angles and are seen more edge-on than other Seyfert 2 galaxies. For this case, the polarization and the contribution of scattered light in the hard component for Seyfert galaxies are naturally explained. We consider two possibilities to explain the viewing angle dependence of $L^{\rm ac}_{2-10}/L_{\rm FIR}$; 1) anisotropic radiation and 2) complex absorption by thick, clumpy clouds. The ASCA data do not provide conclusive results on this issue. This is a subject to future X-ray missions.

The authors acknowledge all member of ASCA team. This research has made use of the NASA/IPAC Extragalactic Database (NED) operated by the Jet Population Laboratory, and of the ASCA archive data base maintained by the ASCA Guest observatory facility at NASA/GSFC. This work is supported by Japan Science and Technology Corporation. YT was financially supported in part by the Ministry of Education, Science, and Culture (Nos. 10044052, and 10304013).

REFERENCES

Antonucci, R. R. J. & Miller, J. S. 1985, ApJ, 297, 621

Appenzeller, I., et al. 1998, ApJS, 117, 319

Awaki, H., Koyama, K., Kunieda, H., & Tawara, Y. 1990, Nature, 346, 544

Awaki, H., Koyama, K., Inoue, H., & Halpern, J.P. 1991, PASJ, 43, 195

Awaki, H. 1999 *Adv. Space Res.*, 23, 837

Bassani, L., et al. 1999, ApJS, 121, 473

Blumenthal, G. R., Keel, W. C., & Miller, J. S. 1982, ApJ, 257, 499

Colbert, E. J. M., Baum, S. A., O'dea, C. P., & Veilleux, S. 1998, ApJ, 496, 786

Comastri, A,. et al. 1998, MNRAS, 295, 443

Dahlem, M., Weaver, K. A., & Heckman, T. M. 1998, ApJS, 118, 401

David, L. P., Jones, C., & Forman, W. 1992, ApJ, 388, 82

Griffiths, R. G., Warwick, R. S., Georgantopoulos, I., Done, C., & Smith, D.A. 1998, MNRAS, 298, 1159

Hayashi, I., et al. 1996, PASJ, 48, 219

Heckman, T. M., et al. 1997, ApJ, 482, 114

Heisler, C. A., Lumsden, S. L., & Bailey,J.A. 1997, Nature, 385, 700

Iwasawa, K., Yaqoob, T., Awaki, H., & Ogasaka, Y. 1994, PASJ, 46, L167

Kallman, T. R. & McCray, R. 1982, ApJS, 50, 263

Kruper, J. S., Urry C. M., & Canizares, C. R. 1990, ApJS, 74, 347

Maiolino, R., & Rieke, G. H. 1995, ApJ, 454, 95

Makishima, K., et al. 1989, PASJ, 41, 697

Matt, G. et al., 1996, MNRAS, 281, L69

Malaguti, G., Bassam, L., & Caroli, E. 1994, ApJS, 94, 517

Malaguti, G., et al. 1998, A&A, 331, 519

Marshall, F., et al. 1992, in Proc of Frontiers of X-ray Astronomy, ed Y.Tanaka, K.Koyama (UAP, Tokyo) p129

Miller, J. S., & Goodrich, R.W. 1990, ApJ, 355, 456

Miyoshi, M., et al. 1995, Nature, 373, 127

Mulchaey, J.S., et al. 1994, ApJ, 436, 586

Murayama, T., Mouri, H., & Taniguchi, Y. 2000, ApJ, in press (astro-ph/9908529)

Mushotzky, R.F. 1982 ApJ, 256, 92

Netzer, H. 1996 ApJ, 473, 781

Netzer, H., Turner,T. J, & George, I. M. 1998 ApJ, 504, 680

Nishiura, S. & Taniguchi, Y. 1998, ApJ, 499, 134

Okada, K. 1998, *Ph.D thesis, University of Tokyo*

Padovani, P. & Rafanelli, P. 1988, A&A, 205, 53

Raymond, J. C. & Smith, B. W. 1977, ApJS, 35, 419

Reynolds, C. S., Fabian, A. C., Makishima, K., Fukazawa, Y., & Tamura, T. 1994, MNRAS, 268, L55

Tanaka, Y., Inoue, H., & Holt, S. S. 1994, PASJ, 46, L37

Tran, H. D., Miller, J. S., & Kay, L. E. 1992, ApJ, 397, 452

Tran, H. D. 1995a, ApJ, 440, 565

Tran, H. D. 1995b, ApJ, 440, 578

Tsuru, T., Awaki, H., Koyama, K., & Ptak, A. 1997, PASJ, 49, 619

Turner, T. J., George, I. M., Nandra, K., & Mushotzky, R. F. 1997b, ApJS,113, 23

Turner, T.J., et al. 1997a, ApJ, 488, 164

Ueno, S., Mushotzky, R. F., Koyama, K., Iwasawa, K., Awaki, H., & Hayashi, I. 1994, PASJ, 46, L71

Ueno, S., Koyama, K., Awaki, H., Hayashi, I., & Blanco, P. R. 1996, PASJ, 48, 389

Ueno, S. 1995 *Ph.D. thesis, Kyoto University*

Ulvestad, J.S. & Wilson, A.S. 1984, ApJ, 278, 544

Weaver, K. A., Yaqoob, T., Holt, S. S., Mushotzky, R. F., Matsuoka, M. & Yamauchi, M. 1994, ApJ, 436, L27

Whittle, M. 1992, ApJS, 79, 49

This 2-column preprint was prepared with the AAS LATEX macros v4.0.

Table 1

observation log

Target Name	Obs.Date	Exp. Time	count rate(SIS)	hardness ratio(2-10/0.5-2)
Was 49b	95. 5.22	43k	0.009±0.001 cts/s	1.5± 0.2
Mrk 348	95.08.04	28k	0.027±0.001 cts/s	8.0± 1.0
Mrk 1210	95.10.18	14k	0.016±0.002 cts/s	1.1± 0.1
	95.11.12	6k	0.017±0.006 cts/s	1.3± 0.4
NGC 7212	95.11.13	16k	0.011±0.001 cts/s	1.2± 0.2
	95.11.19	13k	0.009±0.002 cts/s	0.94±0.2
Mrk 477	95.12.04	30k	0.011±0.001 cts/s	1.6± 0.1
	95.12.05	20k	0.010±0.002 cts/s	1.4± 0.2
Mrk 3	96.10.26	32k	0.047±0.001 cts/s	1.04± 0.04

Table 2

Fitting results for the ASCA spectra.

		Soft Component			Hard Component				
Target	ID[a]	N_{H0} ($\times 10^{22}$ cm^{-2})	Γ/kT −/(keV)	Z	N_{H1} ($\times 10^{22}$ cm^{-2})	Γ	Center Energy (keV)	EW (eV)	χ^2 (d.o.f.)
Was 49b	1	0.85(<1.2)	8.9(2.3–15)	—-	0.16(<0.56)	0.54(0.25–0.9)	5.7(5.4–6.1)	370(200–500)	70.0(62)
	2	0.0163(f)	2.3(0.5–3.0)	—-	6.3(4.5–46)	1.7(f)	6.02(f)	620(370–870)	91.2(65)
	3	0.56(0.2–1.14)	7.2(4–10)	—-	—-	2.8(2.48– 3.12)	6.02(f)	200(<350)	71.4(64)
	4	0.0163(f)	0.72(0.4–1.1)	0.02(<0.14)	1.7(0.7–3.2)	0.6(0.3–0.9)	6.02(f)	360(180–540)	72.0(63)
Mrk 348	1	0.00(<0.24)	1.1(0.5–2.3)	—-	16(13–20)	1.69(1.30– 2.05)	6.27(6.20–6.35)	215(140–300)	117.4(116)
	2	0.056(f)	1.3(0.7–1.9)	—-	16(15–18)	1.7 (f)	6.27(6.20–6.35)	212(140–280)	118.6(119)
	3	0.056 (f)	-3	—-	—-	1.6	4.9	200	242(117)
	4	0.056 (f)	64(6>)	1(f)	16(15–18)	1.64(1.30–2.00)	6.27(6.20–6.35)	215(140–300)	117.6(117)
Mrk 1210	1	0.83(0.16–1.4)	7.3(3.4–10.7)	—-	0.00(<1.7)	-0.14(-0.45– +0.28)	6.29(6.24–6.60)	780(510–1020)	33.2(35)
	2	0.038(f)	2.34(1.90–2.80)	—-	21.1(15–30)	1.7 (f)	6.315(f)	760(430–990)	50.1(38)
	3	0.55(0.1–1.1)	5.6(3.2–8.4)	—-	—-	1.95(1.55–2.40)	6.315(f)	460(250–670)	32.9(36)
	4	0.038(f)	0.86(0.55–1.2)	0.03(<0.1)	3.7(<7.5)	0.08(-0.5–0.5)	6.315(f)	710(440–950)	34.8(36)
NGC 7212	1	0.0(<0.2)	1.37(0.8–4.4)	—-	23(0–200)	0.47(-1.5–10)	6.18(—)[a]	520(—)	30.2(34)
	2	0.0533(f)	1.41(1.0–1.8)	—-	45(20–100)	1.7(f)	6.24(f)	480(<1500)	32.4(37)
	3	0.0533(f)	1.65(0.2–2.3)	—-	—-	1.87(1.35–2.7)	6.24(f)	340(20–700)	30.1(37)
	4	0.0533(f)	12.0(4.5<)	1(f)	25(<95)	0.77(-1.2–5.7)	6.24 (f)	530(60–1200)	32.1(36)
Mrk 477	1	0.0(<0.6)	2.3(1.6–6.5)	—-	4.7(<13)	-0.02(-0.6– +0.6)	6.24(6.27–6.39)	500(350–650)	71.1(70)
	2	0.0127(f)	1.67(1.25–2.1)	—-	30(24–42)	1.7(f)	6.17(f)	300(150–450)	88.3(73)
	3	0.01(<0.32)	2.75(2.1–4.8)	—-	—-	1.57(1.2–1.9)	6.17(f)	230(80–380)	69.7(71)
	4	0.0127(f)	7.5(4.8<)	1(f)	14(6–24)	0.3(-0.4– +2.0)	6.17(f)	340(180–450)	82.4(72)
Mrk 3	1	0.04(<0.09)	1.57(1.41–1.75)	—-	72(50–100)	2.22(1.2–3.3)	6.29(6.27–6.34)	700(520–1100)	148(127)
	2	0.087(f)	1.72(1.60–1.82)	—-	57(48–68)	1.7(f)	6.315(f)	760(590–930)	190.9(130)
	3	0.20(0.12-0.30)	2.47(2.1–2.9)	—-	—-	1.14(0.80–1.48)	6.315(f)	730(610–840)	187.0(128)
	4	0.087(f)	0.98(0.88–1.08)	0.05(0.03–0.09)	0(<0.7)	-0.23(-0.40– -0.04)	6.315(f)	1100(950–1200)	224.3(129)

Note.—ID: (1) absorbed power law plus another absorbed power law model, (2) absorbed power law with photon index of 1.7 plus another power law model, (3) Compton reflection plus absorbed power law model, For reflection models, the reflection mirror has an inclination of $\theta=0^{\circ}$ and a coverage of $\Omega=2\pi$, (4) absorbed power law plus RAYMOND plasma. For Mrk 3, we included a narrow line at $\sim$0.9 keV in the soft component. A fixed parameter is denoted by (f).

[a]Since we did not obtain a significant iron line in this model, its confidence region is too large.

Table 3

Observed X-ray flux and luminosity[a]

Target Name	redshift[b]	X-ray flux (ergs s^{-1} cm^{-2})				X-ray luminosity (ergs s^{-1})	
		soft component		hard component		soft component	hard component
		0.5-2keV	2-10keV	0.5-2keV	2-10keV	0.5-2keV	2-10keV
Was 49b	0.0630	8.6×10^{-14}	3.7×10^{-13}	5.9×10^{-17}	6.3×10^{-13}	1.4×10^{42}	1.0×10^{43}
Mrk 348	0.0149	7.0×10^{-14}	2.8×10^{-13}	2.1×10^{-16}	4.8×10^{-12}	6.3×10^{40}	4.3×10^{42}
Mrk 1210	0.0135	1.8×10^{-13}	1.8×10^{-13}	3.1×10^{-18}	1.4×10^{-12}	1.3×10^{41}	1.0×10^{42}
NGC 7212	0.0260	1.0×10^{-13}	3.3×10^{-13}	5.0×10^{-22}	5.0×10^{-13}	2.8×10^{41}	1.4×10^{42}
Mrk 477	0.0378	1.0×10^{-13}	2.0×10^{-13}	2.6×10^{-19}	1.1×10^{-12}	5.8×10^{41}	6.4×10^{42}
Mrk 3	0.0135	5.8×10^{-13}	1.3×10^{-12}	4.0×10^{-25}	4.2×10^{-12}	4.3×10^{41}	3.1×10^{42}

[a]we listed the flux in the model 2.

[b]Data quated from NASA Extragalactic Database (NED).

Table 4

X-ray, infrared and H_{β}P luminosities for PBL Seyfert 2 galaxies

Target Name	$L^{\rm soft}_{0.5-2}$ [a]	$L^{\rm ac}_{2-10}$ [b]	$L_{\rm FIR}$	$\log(F_{25\mu{\rm m}}/F_{60\mu{\rm m}})$	$L_{{\rm H}_\beta{\rm P}}$	Reference
Was 49b	1.4×10^{42}	2.1×10^{43}	3.5×10^{44}		3.1×10^{40}	1
Mrk 348	7.3×10^{40}	8.0×10^{42}	5.5×10^{43}	-0.19	2.6×10^{39}	1
Mrk 1210	1.4×10^{41}	2.3×10^{42}	5.7×10^{43}	0.04	1.5×10^{39}	1
NGC 7212	3.3×10^{41}	4.9×10^{42}	4.0×10^{44}	-0.57	3.5×10^{39}	1
Mrk 477	6.3×10^{41}	1.8×10^{43}	3.8×10^{44}	-0.41	7.3×10^{39}	1
Mrk 3	6.1×10^{41}	7.0×10^{42}	1.2×10^{44}	-0.11	9.1×10^{39}	1
NGC 1068	3.9×10^{40}	5×10^{41}	5.2×10^{44}	-0.32	2.5×10^{39}	2, 3
Mrk 463E	1.2×10^{42}	8×10^{42}	9.5×10^{44}	-0.14	3.6×10^{40}	1, 4
NGC 7674	4.0×10^{41}	2×10^{42}	6.6×10^{44}	-0.47	4.8×10^{39}	1, 5

[a]the 0.5–2keV luminosity for soft component.

[b]the 2–10 keV absorption corrected luminosity for hard component.

References.— (1) Tran 1995a; (2) Antonucci & Miller 1985; (3) Ueno et al. 1994; (4) Ueno et al. 1996; (5) Malaguti et al. 1998

Table 5

intensity of 0.9 keV structure in model 2

Target Name	center energy	equivalent width
Was 49b	0.85 keV (fixed)	0 (<90)eV
Mrk 348	0.89 keV (fixed)	80 (<240)eV
Mrk 1210	0.89 keV (fixed)	35 (<700)eV
NGC 7212	0.88 keV (fixed)	12 (<120)eV
Mrk 477	0.86 (0.82–0.90) keV	85 (10–160)eV
Mrk 3	0.915 (0.89–0.93) keV	140 (100–200) eV

Table 6

The ratio of $L^{\rm soft}_{0.5-2}/L^{\rm ac}_{0.5-2}$ for PBL Seyfert 2 galaxies and Other Seyfert 2 galaxies

Target Name	$L^{\rm soft}_{0.5-2}/L^{\rm ac}_{0.5-2}$
Was 49b	0.12
Mrk 348	0.017
Mrk 1210	0.11
NGC 7212	0.12
Mrk 477	0.064
Mrk 3	0.16
Mrk 463e[a]	0.273
NGC 7674[b]	0.365
IC 5063[c]	0.014
NGC 4388[c]	0.050
NGC 4507[c]	0.007
IRAS1319-164[c]	0.053
TOL1351-375[c]	0.065
NGC 7172[c]	0.001

References.— (a) Ueno et al. 1996; (b) Malaguti et al. 1998; (c) Ueno 1995.

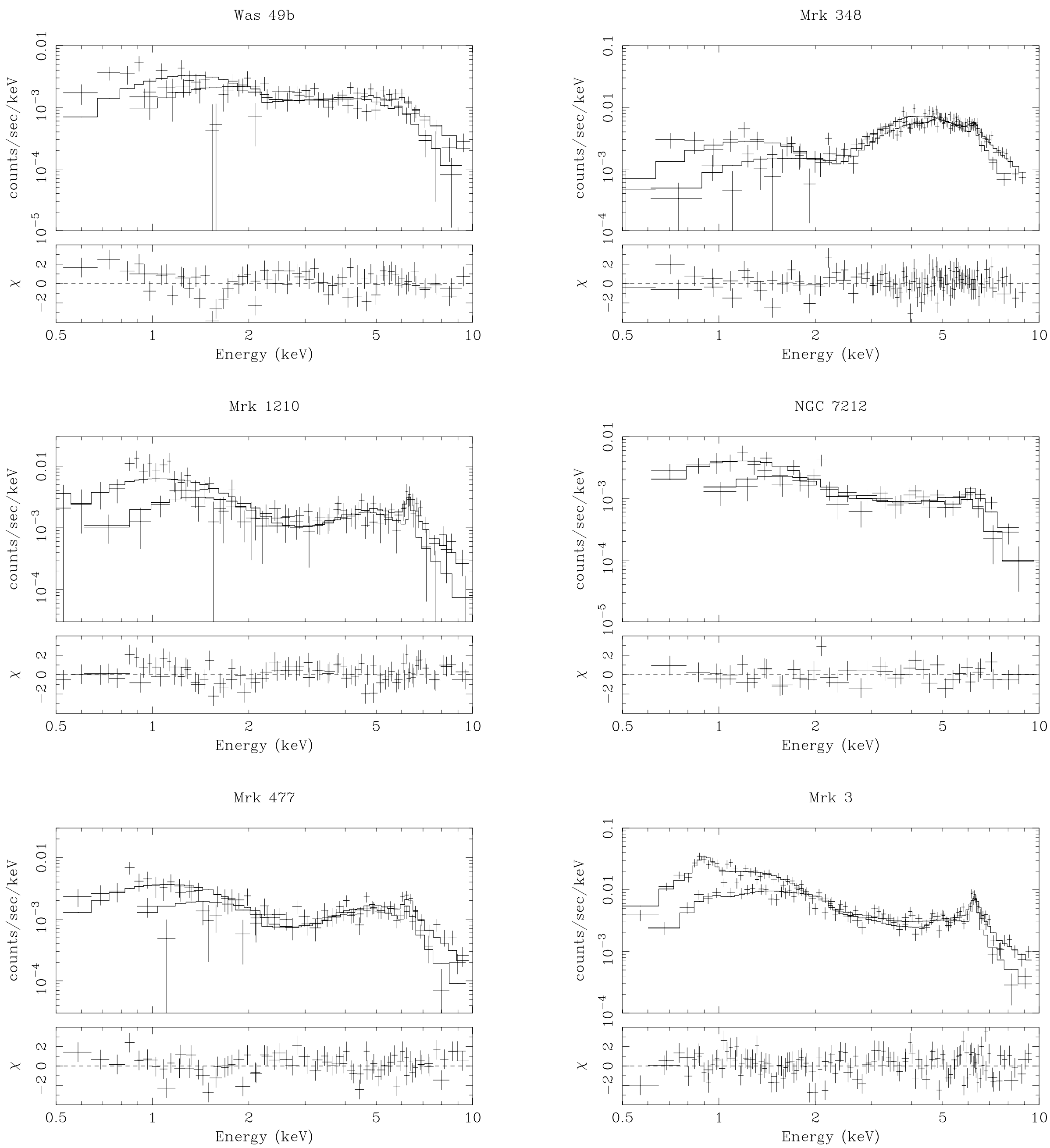

Fig. 1.— ASCA SIS and GIS spectra of Seyfert 2 galaxies with optical polarized broad lines. Histgrams show the best fit models in model 1. Please note that a narrow line at∼0.9keV is included in the spectrum of Mrk 3.

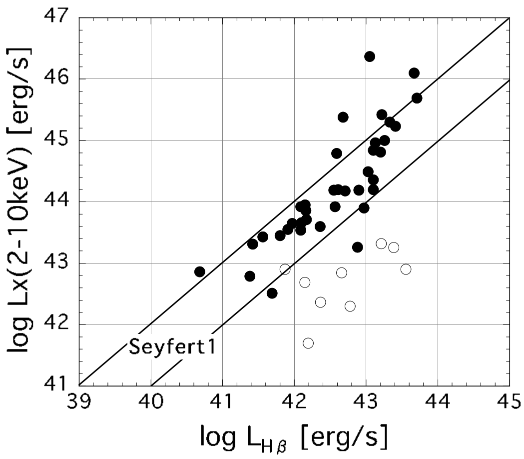

Fig. 2.— Absorption corrected X-ray luminosity ($L^{\rm ac}_{2-10}$) vs. broad Hβ luminosity ($L_{\rm H\beta}$). Closed circles correspond to observations for Seyfert 1 galaxies and QSOs; open circles to estimations for Seyfert 2 galaxies with optical polarized broad lines. Two solid lines show $L^{\rm ac}_{2-10}/L_{\rm H\beta}$ =10 (lower) and 100 (upper).

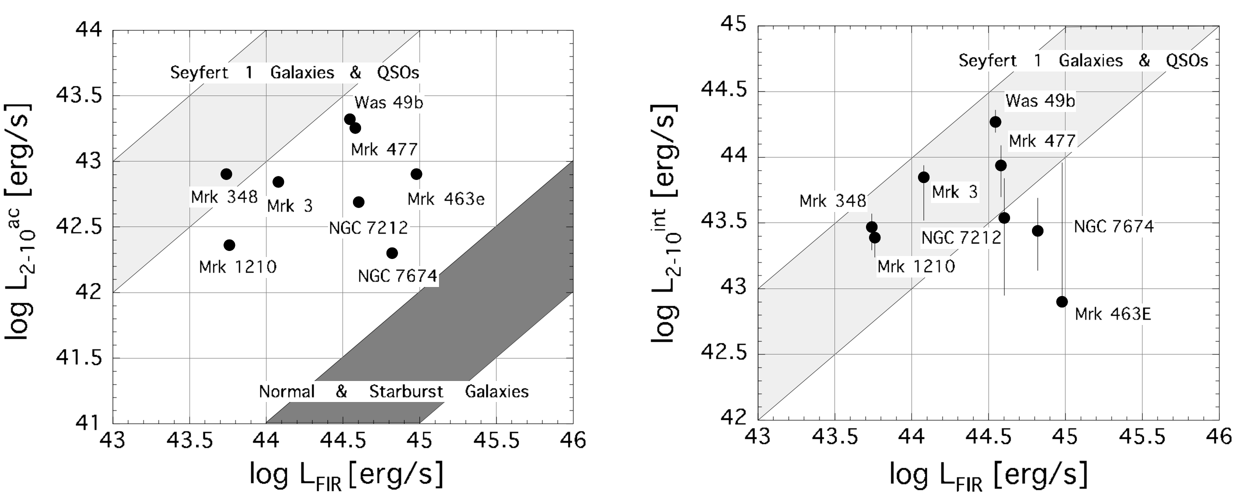

Fig. 3.— Absorption corrected X-ray luminosity ($L^{\rm ac}_{2-10}$) vs. far-infrared luminosity ($L_{\rm FIR}$) (left), and intrinsic luminosity ($L^{\rm intrinsic}_{2-10}$) vs. far-infrared luminosity ($L_{\rm FIR}$)(right). Intrinsic luminosities were estimated from eq. (2) in the text. The regions for normal and starburst galaxies, and Seyfert 1 galaxies and QSOs are also presented in these figures.

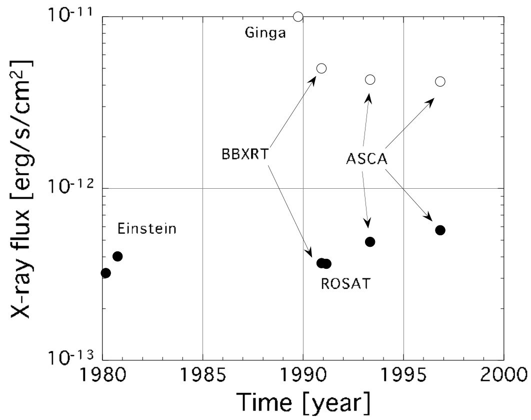

Fig. 4.— Long term monitoring of X-ray flux with various X-ray missions for Mrk 3. Closed circles and open circles show X-ray fluxes in the 0.5 – 2keV and the 2 – 10 keV, respectively.

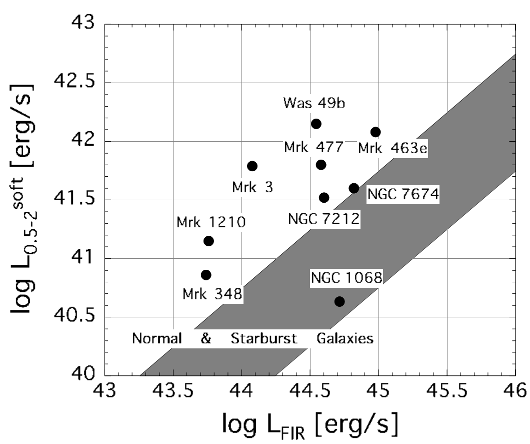

Fig. 5.— The 0.5–2 keV luminosities ($L_{0.5-2}^{\rm soft}$) vs. far-infrared luminosities ($L_{\rm FIR}$). The 0.5–2keV luminosity for NGC 1068 is estimated by extrapolation of the scattered component seen in the 2–10 keV band.

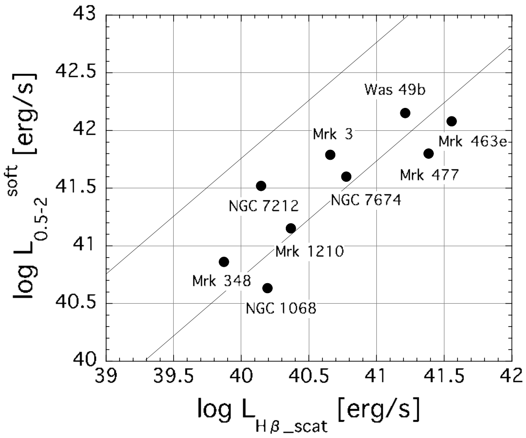

Fig. 6.— The soft X-ray band luminosities ($L_{0.5-2}^{\rm soft}$) vs. the scattered broad Hβ luminosities ($L_{{\rm H}\beta\_{\rm scat}}$). These $L_{{\rm H}\beta\_{\rm scat}}$ are quoted from Tran 1995b and Miller & Goodrich 1990. The two solid lines show $L_{2-10}/L_{{\rm H}\beta}$=10 and 100 assuming a photon index of 1.7.

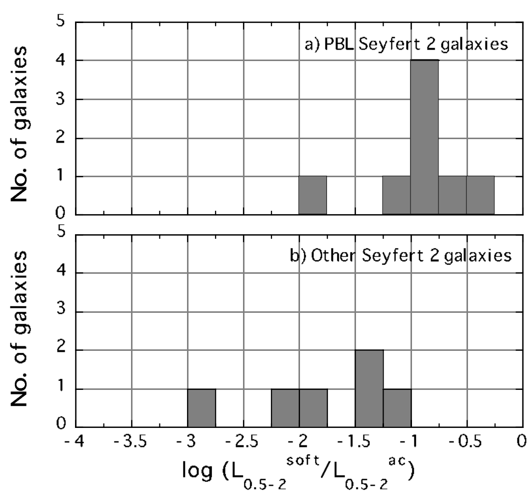

Fig. 7.— Distributions of $L_{0.5-2}^{\rm soft}/L_{0.5-2}^{\rm ac}$ for PBL Seyfert 2 (upper) and for other Seyfert 2 galaxies (lower). The data for other Seyfert 2 galaxies are quated from Ueno (1995).

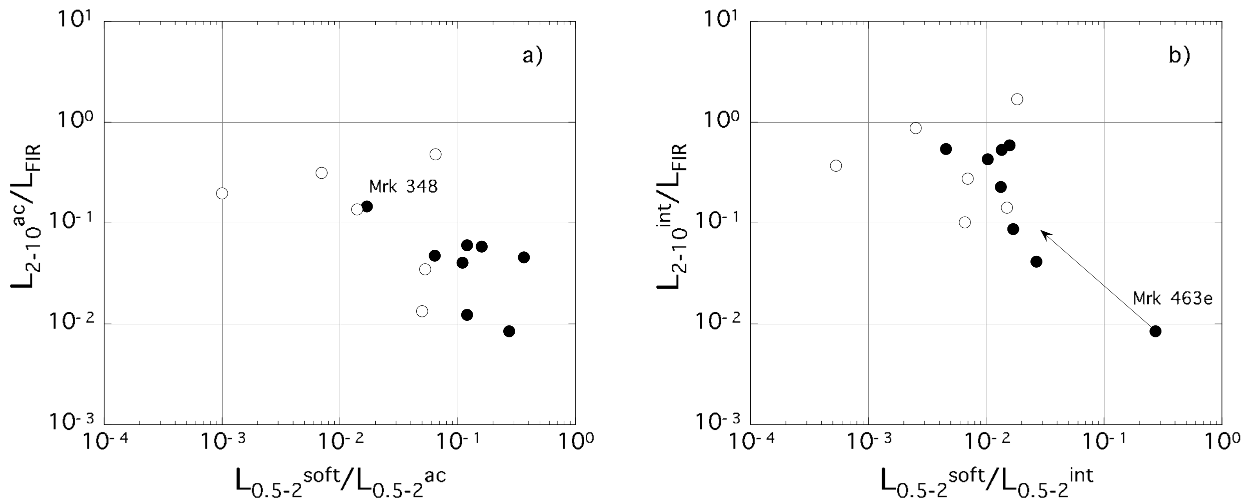

Fig. 8.— $L^{\rm ac}_{2-10}/L_{\rm FIR}$ vs $L^{\rm soft}_{0.5-2}/L^{\rm ac}_{0.5-2}$ (left figure) and $L^{\rm intrinsic}_{2-10}/L_{\rm FIR}$ vs $L^{\rm soft}_{0.5-2}/L^{\rm intrinsic}_{0.5-2}$ (right figure). Closed and open circles display PBL Seyfert 2 and other Seyfert 2 galaxies, respectively. An arrow in figure 8b shows the error region of Mrk 463e.

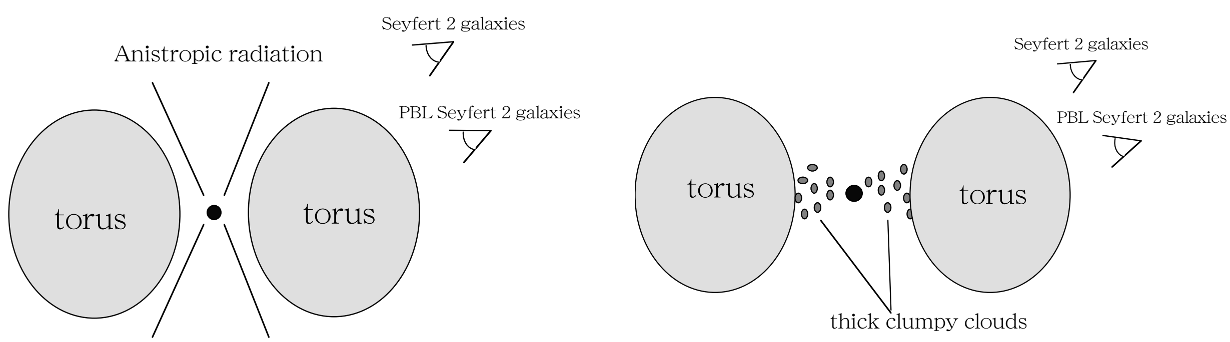

Fig. 9.— Schematic view of Seyfert galaxies proposed in the text. Left and right figures show anistropic radiation model and dual absorption model, respectively.